Chem

Article
Lipid Nanodiscs via Ordered Copolymers

Anton A.A. Smith, Henriette E. Autzen, Bryan Faust, ..., Andrew J. Spakowitz, Yifan Cheng, Eric A. Appel

yifan.cheng@ucsf.edu (Y.C.)
eappel@stanford.edu (E.A.A.)

HIGHLIGHTS
Highly alternating AASTY copolymers are made by controlled radical polymerization

Efficacy of membrane solubilization to nanodiscs with AASTY is dependent on the lipid composition

AASTY copolymers can extract human TRPM4 into native nanodiscs as shown by cryo-EM

The AASTY copolymers offer a route for detergent-free membrane protein extraction

A highly alternating copolymer composed of acrylic acid and styrene (AASTY) is synthesized with controlled radical polymerization by exploiting the reactivity ratios of the monomers to control the monomer sequence. The AASTY copolymers are effective solubilizers of cellular membranes and their embedded proteins, which improves structural characterization by single-particle cryo-electron microscopy (cryo-EM). These copolymers are promising tools for exploring detergent-free membrane protein solubilization and direct formation of native nanodiscs, facilitating structural and functional analysis of the mammalian proteome.

Chem

CellPress

Article

Lipid Nanodiscs via Ordered Copolymers

Anton A.A. Smith,[1,2,10] Henriette E. Autzen,[3,4,10] Bryan Faust,[4] Joseph L. Mann,[1] Benjamin W. Muir,[5] Shaun Howard,[5] Almar Postma,[5] Andrew J. Spakowitz,[1,6] Yifan Cheng,[2,7,*] and Eric A. Appel[1,8,9,11,*]

SUMMARY

Amphiphilic copolymers capable of extracting membrane proteins directly from lipid bilayers into "native nanodiscs" promise a simpler membrane protein sample preparation procedure for structural and functional studies. Unfortunately, the selection of nanodisc-forming copolymers is currently limited to molecules that are heterogeneous in terms of molecular weight and monomer sequence, limiting their efficacy in extracting membrane proteins. Here, we report the development of a highly alternating copolymer composed of acrylic acid and styrene by taking advantage of the fundamental reactivity ratios of these monomers. We show that these copolymers, which we term AASTY, are effective solubilizers of membrane proteins expressed in mammalian cells by virtue of their structured amphiphilicity. These AASTY copolymers are promising alternatives to styrene-maleic acid copolymers and provide a new chemical platform for structural and functional characterization of integral membrane proteins in native nanodiscs.

INTRODUCTION

Integral membrane proteins constitute a major group of therapeutic targets. Their functional characterization and structural determination are fundamental for rational lead discovery in the development of therapeutics. The functional and structural characterization of integral membrane proteins is a rapidly evolving field of research, in large part due to the technological breakthrough of single-particle cryo-electron microscopy (cryo-EM) within the last decade.[1] Without the need of forming well-ordered three-dimensional crystals for structural studies, there is an increasing interest in reconstituting integral membrane proteins in lipid-disc nanoparticles (nanodiscs) that mimic native-like membrane conditions. The dominating approach to embed membrane proteins in nanodiscs is dependent on detergent solubilization and subsequent re-lipidation, inserting the membrane protein into a lipid bilayer encircled by a membrane scaffold protein (MSP) (Figure 1A, white circles).[2] While reconstitution with MSPs enables the study of membrane proteins in a mimic of a lipid environment, the native lipids are lost as they are either partially or fully replaced by a synthetic bilayer, leaving only lipids bound to the target protein with high affinity behind.[3] Moreover, the asymmetry of the membrane is lost in the MSP system. Finally, the detergent-based extraction step may cause destabilization of the protein of interest, and lengthy procedures are required to optimize reconstitution protocols with the appropriate ratios of membrane protein, lipids, and MSPs.

Native nanodisc-forming polymers are amphipathic copolymers capable of dissolving membranes and embedding integral membrane proteins directly from the native lipid bilayer into nanodiscs, circumventing the need for an initial detergent extraction (Figure 1A, blue circles).[4] In contrast to the MSP nanodisc reconstitution

The Bigger Picture

Membrane proteins are mediators between the extra and intracellular milieu and account for a diverse array of physiological functions, making them important diagnostic and therapeutic targets. Unfortunately, isolation of membrane proteins is largely dependent on detergents that may disrupt their structural and functional integrity or hamper biochemical characterization. While industrially used amphiphilic copolymers can extract membrane proteins in native nanodiscs, the composition of these copolymers influences the extraction efficiency. Modern controlled radical polymerization techniques offer structural control for the rational design of copolymers for membrane protein isolation and characterization in native nanodiscs. Copolymers such as AASTY developed here will advance the toolbox for membrane protein isolation by facilitating native conditions outside the cell membrane and be applicable across fields seeking to characterize membrane proteins from natural and recombinant sources.

approach, the native nanodisc method is still in its early stages of development but has shown great promise in cryo-EM and functional characterization on a selection of membrane proteins expressed in *E. coli*[5–7] and mammalian cells.[8–10] However, it is evident from the limited number of studies of membrane proteins embedded in native nanodiscs that the currently available copolymers have several shortcomings.

Styrene-maleic acid (SMA) copolymers, the predominant polymers used in native nanodisc formation applications, are hydrolyzed copolymers of styrene (STY) and maleic anhydride (MAnh) (Figure 1B). These nanodisc-forming copolymers are sensitive to the presence of divalent cations, have a limited effective pH range, and have a broad distribution of molecular weights due to the nature of the synthesis.[11] Moreover, nanodiscs formed with SMA copolymers have a low affinity to matrices used in affinity-based purification methods, such as Ni-NTA or Strep-Tactin, compromising protein purification procedures. The reduced affinity is likely due to charge-repulsive effects as the issue can be ameliorated by either increasing the salt concentration or including positively charged compounds, such as L-arginine or glycine in the binding buffer.[4,10]

The main innovations in the development of more effective nanodisc-forming copolymers have focused on modifying SMA with functional groups using commercial SMAnh as the starting material. Examples include poly(styrene-co-maleimide) and various amine-modified SMA copolymers, rendering the resulting discs stable at low pH and insensitive to divalent cations.[12–17] Other polymers such as poly(diisobutylene-co-maleic acid) (DIBMA) and random polymethacrylate copolymers that are more resistant to divalent cations than SMA have emerged as promising alternative candidate polymers.[18,19] However, the field is limited in terms of controlling the monomer sequence distribution, and molecular weights, an innate limitation in the synthesis of SMA due to the reactivity ratios of STY and MAnh.[20–22]

The most generally used SMA copolymers have a ratio of STY to MA of 2:1.[11] Their use for characterizing membrane proteins were recently reviewed elsewhere.[23,24] The copolymerization of STY and maleic anhydride (MAnh) is close to perfectly alternating, which makes the batch synthesis of 2:1 copolymers impossible.[25] To obtain the 2:1 STY:MAnh precursor copolymer, it is necessary to have an approximately 20-fold stoichiometric excess of STY with respect to MAnh throughout the reaction. Consequently, 2:1 SMAnh is made in continually stirring tank reactors where a continuous feed of the reactants achieves a steady-state polymerization that results in a 2:1 ratio. In the monomer consumption, which results in a non-random statistical distribution of STY and MAnh along the chain.[26] Since these protocols use the traditional free radical polymerization, the polymers that are formed exhibit high disparities in molecular weight (Figure 1C). While SMAnh can also be made through reversible addition-fragmentation chain-transfer (RAFT) polymerizations, the resulting polymers obtain a steep gradient in the monomer composition along the chain, if it deviates from the azeotropic monomer composition of approximately 1:1 STY to MAnh. Since the functional SMA copolymers have a composition of 2:1 STY to MA, batch RAFT copolymerizations of this composition are not possible without forming a gradient.[21]

We hypothesized that poly(acrylic acid-co-styrene) (AASTY) copolymers may act as effective nanodisc-forming polymers on account of their structural similarity to SMA (i.e., they both contain STY and carboxylate functionalities) and their highly alternating behavior due to the reactivity ratios between STY and AA in radical polymerizations (Figure 1B).[27] Poly(acrylic acid) derivatives were among the first

[1]Department Department of Materials Science and Engineering, Stanford University, Stanford, CA 94305, USA

[2]Department of Health Technology, Technical University of Denmark, 2800 Kongens Lyngby, Denmark

[3]Section of Biomolecular Sciences, Department of Biology, University of Copenhagen, Denmark

[4]Department of Biochemistry and Biophysics, University of California, San Francisco, San Francisco, CA 94158-2517, USA

[5]CSIRO Manufacturing, CSIRO, Clayton, VIC 3168, Australia

[6]Department of Chemical Engineering, Stanford University, Stanford, CA 94305, USA

[7]Howard Hughes Medical Institute, University of California, San Francisco, San Francisco, CA 94158-2517, USA
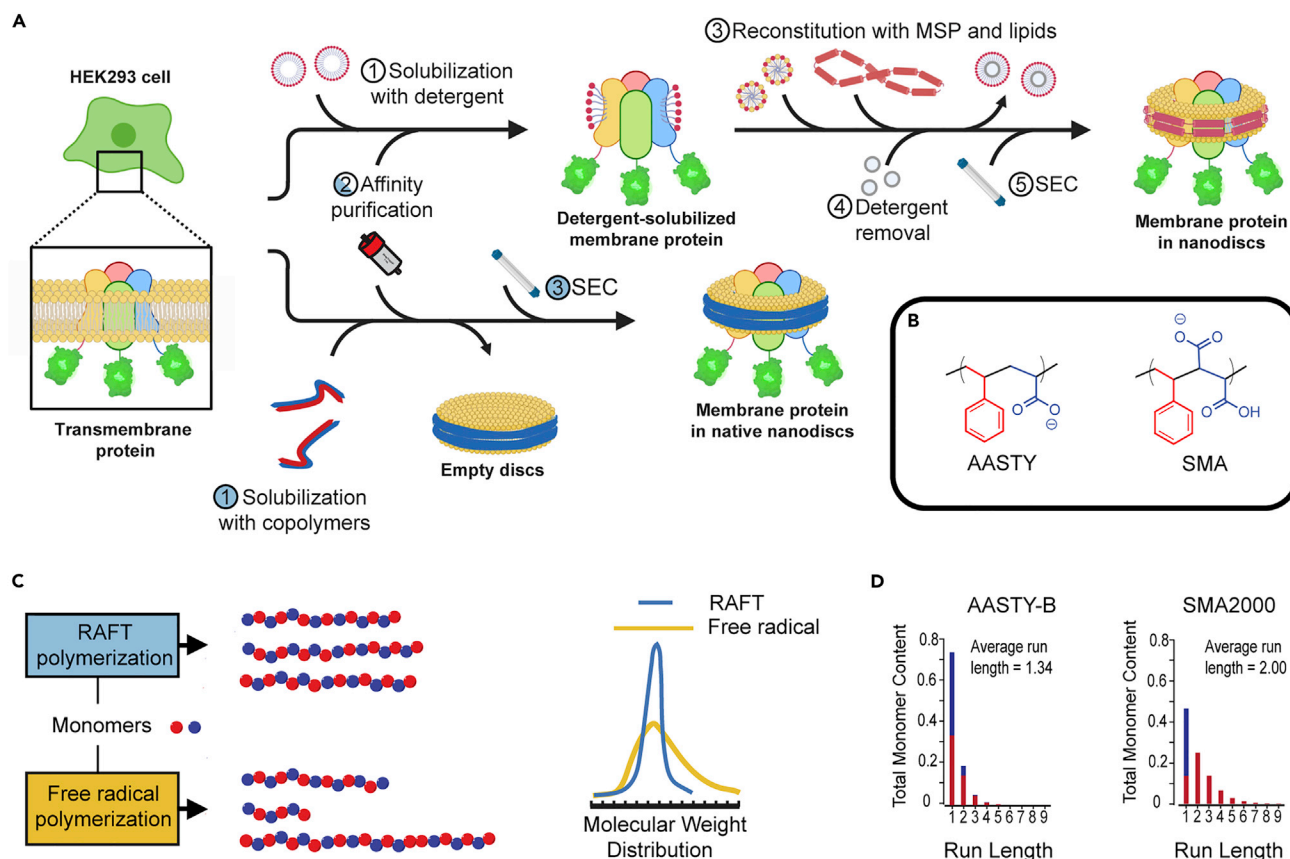
[8]Department of Bioengineering, Stanford University, Stanford, CA 94305, USA

[9]ChEM-H Institute, Stanford University, Stanford, CA 94305, USA

[10]These authors contributed equally

[11]Lead Contact

*Correspondence: yifan.cheng@ucsf.edu (Y.C.), eappel@stanford.edu (E.A.A.)

https://doi.org/10.1016/j.chempr.2020.08.004

Chem
Article

 CellPress

Figure 1. Overview of Membrane Mimetics Systems and Features of RAFT AASTY Copolymers

(A) Protein overexpressed in mammalian cells are typically purified using detergents and reconstituted into lipid bilayers with belt forming proteins (steps 1–5, white circles). First cells are treated with detergent (step 1), followed by purification of the recombinant protein in detergent micelles by affinity chromatography (step 2). The detergent-solubilized, purified protein is then reconstituted into a lipid bilayer by adding detergent-solubilized lipids and MSP (step 3), and detergent is removed with bio-beads (step 4). Finally, aggregates and/or empty discs are then removed by SEC (step 5). Alternatively, membrane proteins can be purified with amphiphilic copolymers and put directly into a nanodisc (steps 1–3, blue boxes). First, cells are incubated with the copolymer (step 1), during which the native nanodiscs spontaneously form. Next, the protein in native nanodiscs is purified by affinity chromatography (step 2) and SEC (step 3).

(B) The AASTY copolymer is composed of STY and AA. SMA2000, the most commonly used copolymer for native nanodisc preparations, is composed of STY and MA.

(C) The AASTY copolymers are synthesized using RAFT making them more homogeneous than copolymers synthesized through traditional radical polymerization.

(D) SMA has a statistical distribution of monomers along the copolymer chain, with the possibility of multiple STY appearing in sequence. Averaging the statistical distribution of both monomers gives AASTY an average homomonomer run-length of 1.34, while SMA2000 has a run-length of 2.0. Thus, the AASTY copolymers present a more alternating sequence than SMA2000, giving it a more regular structure of the two. See also Table S1.

polymers developed for stabilizing membrane proteins, initially as micelle forming amphipols, and recently as nanodisc-forming polymers.[28,29] The poly(acrylic acid) derivatives all share a statistical distribution of hydrophobic moieties as a consequence of their post-polymerization functionalization, whereas AASTY copolymerization inherently introduces a highly alternating structure. Similar to SMAnh, AASTY copolymers also form gradients in RAFT copolymerizations, but the gradients are shallower than those arising in SMAnh for the desired compositions of AASTY, which are closer to 1:1 STY to AA. As such, the reactivity ratios of STY and AA facilitate the synthesis of the desired monomer distribution. Additionally, RAFT allows control of the molecular weight and dispersity of the copolymer. Here, we report the use of the AASTY copolymer to isolate a human ion channel from mammalian cells and

Table 1. Copolymer Characteristics

	Initial AA	Conv.%	AA Cont.	Λ	M_n kDa (SEC)	Đ
A	0.40	0.65	0.44	−0.69	6.6	1.19
B	0.45	0.96	0.45	−0.72	8.9	1.21
C	0.50	0.95	0.48	−0.76	8.0	1.20
D	0.55	0.93	0.52	−0.73	7.4	1.14

Acrylic acid, AA; Conv, conversion; acrylic acid content, AA Cont.

demonstrate the potential of using this copolymer in the structural determination of membrane proteins in a native lipid environment by single-particle cryo-EM.
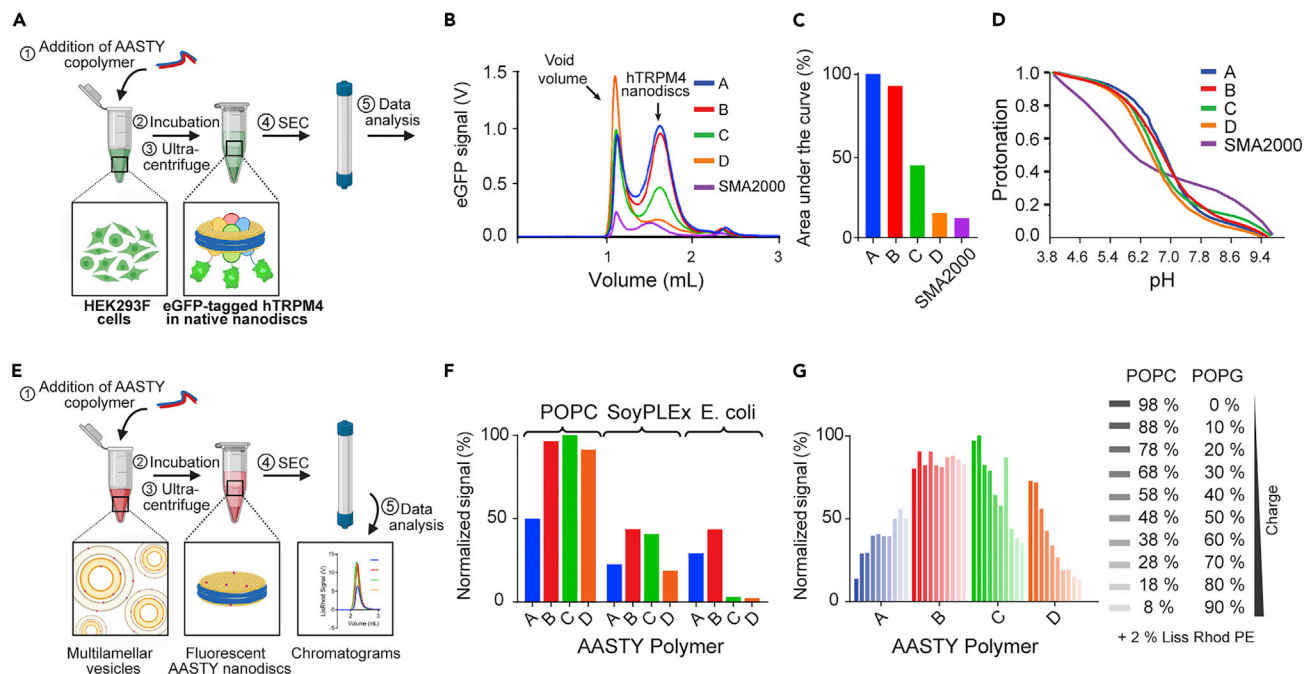
RESULTS AND DISCUSSION

AASTY Solubilizes the hTRPM$_4$ Ion Channel from HEK293 Cells

Based on an initial screen of copolymer compositions, we synthesized four AASTY copolymers (A–D) with a narrow range of compositions limiting the starting AA monomer fraction to 40%–55% and the molecular weight to 6–8 kDa, a molecular weight range that has proven optimal for other acrylic nanodisc-forming polymers (Table 1).[30]

There is currently no standardized metric to compare the nanodisc formation efficacy. This is further complicated by the observation that polymer extraction is largely protein and lipid dependent, with nanodisc-forming polymers being equal, more, or less effective than the detergent, dependent on the system.[31–35,58,59] Polymers for which there exists comparisons of extraction efficacies to SMA2000 are outlined in Table S1, in addition to known limitations in buffer compatibilities and divalent cations. In this study, we assessed the efficacy of AASTY polymers with fluorescent size-exclusion chromatography (FSEC), using HEK293F cells recombinantly overexpressing the human transient receptor potential melastatin type 4 (hTRPM4) fused with an N-terminal StrepTagII and a green fluorescent protein (GFP) tag as our test system (Figure 2A). hTRPM4 is well expressed in HEK293 cells and we previously solved two high-resolution structures of hTRPM4 reconstituted in MSP2N2 nanodiscs with single-particle cryo-EM, showing that this is a membrane protein amenable for structural analysis.[36]

According to the FSEC traces, the protein-containing AASTY nanodiscs were all consistently smaller than those produced by SMA2000, which may be a result of their more regular polymer structure, allowing for a more regular interaction pattern between the polymer and the lipid bilayer. FSEC traces with hTRPM4 indicate that all four AASTY polymers can extract hTRPM4 in discs, albeit with a portion of the protein appearing in the void volume (Figure 2B). Quantification of the peak corresponding to the properly folded protein indicates that polymers A and B are nearly 5 folds more efficient than SMA2000 (Figure 2C). For comparison, AASTY-A and AASTY-B solubilize hTRPM4 about as efficiently as the detergent mixture of n-dodecyl-B-D-maltoside (DDM) and cholesteryl hemisuccinate (CHS) used by Autzen et al. (Figure S2).[36]

The Bjerrum plot of the polymers was measured to characterize the ionization, and the polymers were found to only have a single pK_a value, spanning a relatively short pH range, as opposed to SMA, which has two pK_a values, due to the vicinal dicarboxylate of the maleic acid monomer (Figure 2D). The lower degree of protonation at pH ≈ 7.5 also suggests that AASTY could be effective at lower pH, whereas SMA benefits from a more alkaline pH.[37] The structural differences between AA and

Figure 2. Solubilization of hTRPM4 and Formation of Empty Discs

(A) Schematic of preparation of hTRPM4 loaded native nanodiscs from HEK293 cell lysate, illustrating the five general steps of the preparation of protein-loaded nanodiscs.

(B) Raw FSEC traces from solubilizing the eGFP-tagged hTRPM4 with AASTY and SMA2000 copolymers. The void volume and the peak with properly folded protein are marked with arrows.

(C) Normalized max peak values of the protein peak corresponding to hTRPM4 in native nanodiscs from the FSEC traces in (B) to better illustrate the differences in efficiency.

(D) Bjerrum diagram of the AASTY and SMA2000 copolymers for characterization of their pK_a, and corresponding tolerance to low pH.

(E) Schematic of preparation of empty native nanodiscs from hydrated lipid films, illustrating the five general steps of the preparation of protein-free nanodiscs.

(F) Max peak values of the empty nanodisc FSEC traces with POPC, Soy plex, and *E. coli* lipid mixed with 2% Liss Rhod PE. Values are normalized relative to the highest detected signal for the contained data.

(G) Maximum fluorescence signals from FSEC with polymers A, B, C, and D and various ratios of POPC and POPG lipids and 2% Liss Rhod PE with an overall increase in the content of POPG and thereby negative charge. Values are normalized relative to the highest detected signal of the contained data. See also Figures S2 and S3.

MA also translate into reduced sensitivity to divalent cations for AASTY compared with SMA, as AASTY discs are stable up to 7 mM Ca^{2+}, as opposed to SMA discs which become unstable above 2 mM (data not shown).[37] This observation is consistent with the severely reduced solubility of vicinal dicarboxylate species with Ca^{2+}, as compared with other dicarboxylate chelators.[38,39]

Lipid Dependency on Protein-Free Nanodisc Formation

Previous studies of SMA copolymers report no solubilization preference toward specific types of lipids.[40–42] To determine whether the lipid composition has an effect on the solubilization efficiency of AASTY copolymers, we formed protein-free AASTY-stabilized nanodiscs incorporating 2% of the fluorescent Lissamine Rhodamine B (Liss Rhod) phosphatidylethanolamine (PE) lipid with three different lipid mixtures: (1) 1-palmitoyl-2-oleoyl-glycero-3-phosphocholine (POPC), (2) soy polar lipid extract (PLEx), and (3) *E. coli* PLEx and analyzed the discs by FSEC (Figure 2E). The protein-free nanodiscs were formed by incubating 1% polymer with a 1 mM suspension of cleared, multilaminar lipid vesicles in the buffer for 2 h. The solubilization efficiency was evaluated based on fluorescence intensity with FSEC after an ultracentrifugation

Chem
Article

step to remove insoluble materials and visually inspection of the pellets in the ultra-centrifugation tubes. With well-documented lipid compositions from the manufacturer, the synthetic and extracted lipid mixtures provide a controlled platform for examining the polymer-lipid effects compared with using isolated cell membranes with various amounts of endogenous proteins.

The synthetic, zwitterionic lipid POPC forms nanodiscs with all four polymers tested, with AASTY-A being the least effective based on the FSEC traces (Figure 2F). Soy PLEx also forms nanodiscs with all four polymers but is significantly less soluble than POPC, producing a large insoluble fraction after ultracentrifugation compared with POPC. Based on FSEC traces, AASTY-B and -C are better at producing protein-free discs than A and D (Figure 2F). *E. coli* PLEx forms nanodiscs with AASTY-A and -B with the same efficiency as for Soy PLEx but not C and D. We speculate that these differences in solubility between POPC, Soy PLEx, and *E. coli* PLEx originate from the negatively charged lipid species present in the mixtures: In Soy PLEx, phosphatidylinositol (PI) represents ~18% of the lipid species, while in *E. coli* PLEx. phosphatidylglycerol (PG) and cardiolipin constitute ~23% and ~10%, respectively.

To investigate the possible influence of charge on the efficiency of the nanodisc formation further, the synthetic variant of PG, 1-palmitoyl-2-oleoyl-sn-glycero-3-phospho-(1'-rac-glycerol) (POPG), was systematically varied, together with POPC in ten different ratios with a constant 2% Liss Rhod PE and allowed to form nanodiscs with the AASTY copolymers (Figure 2G). According to these experiments, AASTY-B is equally capable of forming nanodiscs across all the tested POPC to POPG ratios, while nanodisc formation with AASTY-A is more efficient when increasing the amount of the negatively charged POPG, and less efficient with AASTY-C and -D with an increase in negative charge (Figure 2G). The solubilization differences between the AASTY copolymers are pronounced, considering the modest differences in their composition (Table 1).

Next, we investigated the effect of cholesterol, the major sterol in mammalian cells that has a significant influence on the physical properties of membranes, particularly through decreasing its fluidity.[43] In a pure POPC system with a constant 2% Liss Rhod PE, we systematically varied the POPC and cholesterol content with up to 50% cholesterol as this is the reported upper bound for some mammalian membranes, while the typical plasma membrane is composed by 10%–30% cholesterol.[44] For all four AASTY copolymers, increasing the cholesterol content decreased the efficiency of nanodisc formation overall, with ranges 30%–50% being particularly destructive (Figure S3). Notably, AASTY-A and AASTY-D were least efficient but showed less variability than AASTY-B and -C when going from 0% to 10% cholesterol. Altogether, the efficiency of forming nanodiscs with the AASTY copolymers is not only dependent on membrane charge but also the sterol content or fluidity, further supporting the notion that nanodisc formation is protein and lipid dependent.

Copolymer Characteristics Influencing Solubilization

According to solubilization experiments of HEK293F cells expressing hTRPM4 and FSEC of the crude lysate, AASTY-A and -B are the most effective at solubilizing hTRPM4 (Figures 2B and 2C). The fact that AASTY-B is the best nanodisc-forming polymer is further supported by the protein-free nanodisc data (Figures 2F and 2G). With a composition of 45:55 of AA to STY, AASTY-B was the most effective solubilizing polymer across all the tested lipid compositions and seems less dependent on lipid charge than AASTY-A, -C, and -D. We hypothesize that the effectiveness of

Chem
Article

CellPress

AASTY-B arises from the optimum overall ratio of AA to STY, which is also the azeo-tropic composition (Table 1; Figure S1). The three other polymers have a mild gradient (Figure S1), and it is unknown if this has an influence on the system. We attri-bute the overall superior solubilization effectiveness of the AASTY polymers compared with SMA2000 to the highly alternating distribution of STY to carboxylate pendant groups along the polymer backbone, while also having a molecular weight in the optimum range (Table 1; Figure S1). SMA2000 has a broad dispersity index, and while it has been shown that nanodiscs form across all polymers masses, the frac-tion around 7 kDa forms more stable nanodiscs.[45] AASTY RAFT copolymerization al-lows targeting this molecular weight, while retaining a low dispersity.

The solubilization profiles of AASTY-C and -D indicate that a deviation in AA content from that observed in AASTY-B is detrimental to the functional nanodisc formation (Figure 2G). Furthermore, the lipid composition that each polymer most effectively solubilizes mirrors the polymer composition in terms of charge, where polymers with increased AA content are most effective in solubilizing zwitterionic lipid composi-tions. To further understand the influence of the polymer sequence, we applied the zero-order Markov model to the simulation output of compositional drift and calculated the chemical correlation parameter, λ, yielding a numerical measure of the monomer sequence.[46,47] For reference, $\lambda = 0$ is a perfectly random copolymer, $\lambda = -1$ is a perfectly alternating copolymer, and $\lambda = 1$ is a di-block copolymer with equal DP in blocks. AASTY-B, -C, and -D all have a $\lambda < -0.70\%$, and more than 70% of all monomers are of the run-length 1 (i.e., these copolymers are more than 70% alternating) (Table 1; Figure S1). Polymer C was the most alternating copolymer, with a $\lambda = -0.76$, and it should be expected to be the most effective copolymer if regularity was the most dominating factor. This is not the case, which suggests that the ratio of carboxylate to STY is more crucial for lipid solubilization. Interestingly, the polymer that is most effective, AASTY-B, is the one with the least amount of gradient formation. This copolymer was polymerized closest to the azeotropic monomer composition (where the copolymer composition is identical to the monomer composition during polymerization regardless of conversion). While less alternating than AASTY-C, AASTY-B is without a gradient, and thus, has the most homogeneous monomer composition along the chain.

hTRPM4 Purification and cryo-EM Imaging

Based on the FSEC results, we purified hTRPM4 in AASTY-B, following a protocol similar to that with DDM and CHS described by Autzen et al.[36] We found that hTRPM4 in native nanodiscs was only retained on affinity resins when including 250 mM L-arginine in the binding and elution buffers (Figures 3A and 3B). We then analyzed the peak fraction with single-particle cryo-EM. The sample is hetero-geneous despite its high purity, with only a few uniform particles with the expected morphology per micrograph (Figure 3C). However, 2D class averages of the most uniform particles show high similarity to those of hTRPM4 in MSP2N2 nanodiscs, confirming that AASTY-B indeed stabilizes hTRPM4 in a nanodisc (Figure 3D).[36] The particles of hTRPM4 in the AASTY-B nanodisc are of insufficient quality to yield a high-resolution structure, but the overall shape of the ~18 nm 3D envelope con-firms that hTRPM4 is stabilized in a polymer nanodisc (Figure 3E). We suspected that the sample heterogeneity in ice was due to aggregation of the highly anionic sample at the air-water interface, as the sample on grids with layers of graphene ox-ide (GO) functionalized with amine appears to be more homogeneous (Figure S4). However, particles on GO grids yielded inferior looking 2D class averages compared with holey carbon grids. Together, the cryo-EM studies suggest that hTRPM4 is conformationally heterogeneous in AASTY-B nanodiscs. This suggestion is further
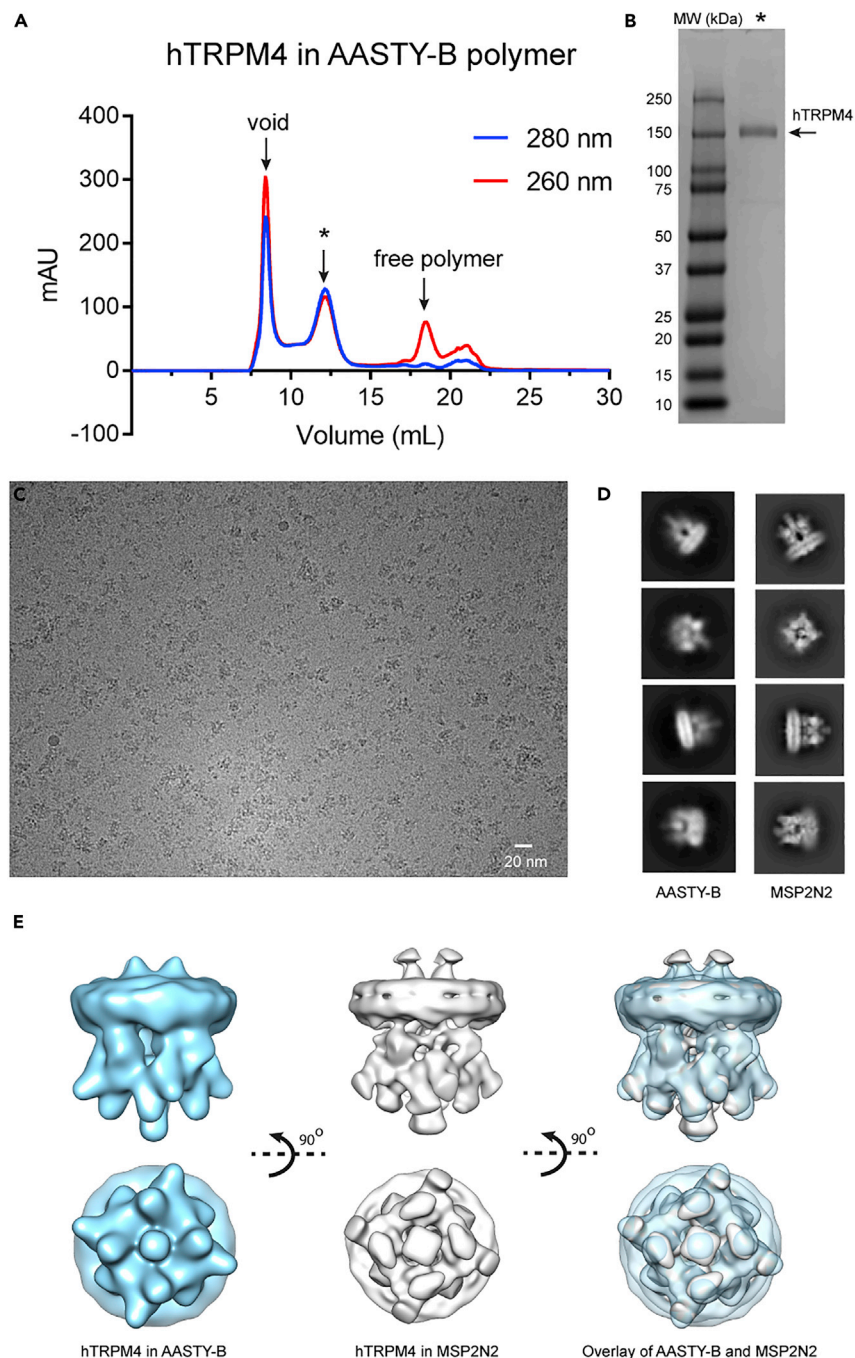
Figure 3. Purification and Single-Particle cryo-EM of hTRPM4 in AASTY-B

(A) SEC traces of purified hTRPM4 at 260 and 280 nm with labeled peaks.

(B) SDS-PAGE of purified hTRPM4 from the main peak in a. Molecular weight bands and hTRPM4 are noted. The remaining gel lanes on the right of the two showed lanes were omitted due to irrelevance.

(C) Example of a cryo-EM micrograph of hTRPM4 in AASTY-B nanodiscs with a 20 nm scale bar.

(D) 2D class averages of hTRPM4 in AASTY-B and MSP2N2 described in Hardy et al.,[31] showing similar views observed in the two samples. The MSP approach is well-studied and currently the preferred route for enabling structural and functional studies of membrane proteins in a lipid environment.

(E) 3D reconstructions of hTRPM4 in AASTY-B (left) and MSP2N2 low-pass filtered to 18 Å (middle) and the two superimposed (right). See also Figure S4.

Chem
Article

CellPress

supported by the observation that hTRPM4 is likely dependent on CHS to be conformationally stabilized to yield high-resolution structures.[48–50] Attempts to extract hTRPM4 in AASTY nanodiscs in the presence of CHS yielded micrographs with particles looking as heterogeneous as in its absence, and 2D class averages that looked worse than without CHS. We suspect that CHS is not a replacement for cholesterol as also suggested by simulation studies comparing the two strolls.[51] Thus, high-resolution cryo-EM structures of membrane proteins as those of hTRPM4 may not necessarily indicate that they are stabilized by cholesterol, but merely that they need a bulky molecule to stabilize them in a minimum.

Conclusions

In summary, we present the development of AASTY, a nanodisc-forming copolymer composed by AA and STY. As a proof of concept, we show that the AASTY copolymer is capable of extracting hTRPM4 into native nanodiscs from mammalian cells and that the technique shows promise in single-particle cryo-EM on human, integral membrane proteins. The AASTY polymer is synthesized using RAFT polymerization, which provides control of the molecular weight, dispersity, and the monomer gradient within the copolymer. The chemical composition using AA rather than MA in combination with control of the monomer gradient increases the fraction of functional membrane-solubilizing copolymer compared with the SMA2000 copolymer conventionally used for forming native nanodiscs. In addition to the charge of the membrane, we speculate that the overall charge of the membrane protein itself influences the extraction efficiency with polyanionic copolymers, such as AASTY and SMA. A charge effect warrants screening copolymers of differential compositions, such as AASTY A–D presented here, and continue the development of neutral polymers. Nevertheless, the AASTY copolymer is a promising alternative to the conventionally used SMA copolymers for structural and functional studies of membrane proteins in native nanodiscs.

EXPERIMENTAL PROCEDURES

Resource Availability

Lead Contact

Further information and requests for resources and reagents should be directed to and will be fulfilled by the Lead Contact, Eric A. Appel (eappel@stanford.edu).

Materials Availability

There are restrictions to the availability of the AASTY polymers designed for this study due to the scale of synthesis. Furthermore, an MTA is required.

Data and Code Availability

Data generated for this study have not been deposited to any repositories but is available upon request.

Method Details

Synthesis of AASTY Copolymers

Copolymerizations were performed neat, with azobisisobuntyrunitrile (AIBN) as initiator, using 2-cyano-2-propyl dodecyl trithiocarbonate (2-CPDT) as the RAFT chain-transfer agent (CTA), resulting in a dodecyltrithiocarbonate end group. The ratios of styrene and acrylic acid were varied, as denoted in Table 1. The polymerizations were performed neat, at [M]/[2-CPDT] of 92. Copolymers were made by parallel automated synthesis as described below. Due to the solvent-free conditions and generally high conversions, the products had high viscosities or were solid. The crude reaction mixtures were diluted or dissolved in acetone, and the copolymers were precipitated into diethylether, and the precipitate collected by filtration and

dried *in vacuo*. Large-scale parallel syntheses of copolymers were conducted on a Chemspeed SLTII automated synthesizer. The reactions were performed in 100 mL disposable ISynth reactors fitted with actively cooled reflux-condenser lids, and mixing was accomplished by vortex agitation. Temperature control was maintained by the use of a Huber cryostat with an operational range of −20°C–150°C. All aspirations and dispensing of reagent solutions were performed using a 4-Needle Head tool equipped with 2 × 1 and 2 × 10 mL syringes, with only the 10 mL syringes used in this particular experiment. All solvent lines were primed with 60 mL (6 strokes of syringe volume) of degassed dimethylformamide. Typical aspiration and dispense rates of the reagents were 5 and 10 mL/min, respectively, for the 10 mL syringes. An air gap of 50 μL and an extra volume of 50 μL were used for all aspirations using the 4-Needle Head tool, and needles were rinsed after each reagent dispense task with a 30 mL inside and 30 mL outside the volume of the priming solvent. The dimethylformamide reservoir was degassed by continuous nitrogen sparging. All stock solutions, including freshly distilled styrene, acrylic acid, and a combined solution of 2-CPDT (250 mg/mL) and AIBN (23 mg/mL) in styrene, were prepared in 60 mL septa-capped reagent vials. These stock solutions were degassed by sparging with argon for 15 min before transfer into the Chemspeed. The atmosphere within the Chemspeed was reduced to less than 1% oxygen by purging with nitrogen while exhaust ports were closed. Reactors were set to open under nitrogen flow until the start of the reaction. The desired aliquots of stock solutions and solvent from the reservoir were transferred to the reactors with the automated liquid handling system before the reactors were set to closed independent and were heated to 60°C and vortex mixing of 400 rpm. Temperature control and mixing were continued for the full 5 h duration of the reaction, at which time the temperature was rapidly dropped to 20°C. The dodecyltrithiocarbonate end groups were removed with H_2O_2 according to a modified procedure by Jesson et al.[52] Copolymer (5 g) was dissolved in a 1:3 mixture of water:ethanol (40 mL) and 30% H_2O_2 (1.8 mL) was added, and the mixture was incubated at 70°C overnight, or until colorless. At this elevated temperature, the polymer is completely soluble but will undergo liquid-liquid phase separation at room temperature. The resulting biphasic solution was split into two 50 mL centrifuge tubes, and the copolymer was precipitated by the addition of water. The precipitated copolymer was collected by centrifugation, the supernatant was discarded, and the isolated copolymer was subsequently dried *in vacuo*. The solid was dissolved in diethyl ether, and precipitated into hexane, and dried under high vacuum. The copolymers were then converted into their sodium salts by dropwise addition of a 1 M NaOH solution to a solution of the copolymer in a 1:1 EtOH:water mixture until pH reached 7.6. Any residual particulate matter was removed by filtration through a 0.22 μm nylon syringe filter, and the resulting solutions were freeze dried to recover final copolymer salts as a white solid. Number-average (M_n) and weight-average (M_w) molar mass and the dispersity (Đ = M_w/M_n) of polymers were obtained using size-exclusion chromatography (SEC) carried out using a Dionex Ultimate 3000 instrument (including pump, autosampler, and column compartment) outfitted with a Dawn Heleos II Multi Angle Light Scattering detector, and a Optilab rEX refractive index detector. The column was a Superose 6 Increase 10/300 from GE Life Sciences (GL). Data were analyzed using Astra 6.0 software. A dn/dc of 0.170 mL/g was used for all samples. A Varian Inova 300 MHz NMR instrument was used to acquire 1H-NMR. The polymers were all analyzed with the compositional drift tool.[46]

Preparation of Protein-Free Nanodiscs

Several different lipid compositions were assessed on FSEC using 2% (w/v) Liss Rhod PE (Avanti Polar Lipids Cat# 810158) as the fluorophore. In general, lipids dissolved

Chem
Article

in chloroform were transferred and dried in glass tubes under a gaseous nitrogen stream. Next, the tubes were wrapped in Parafilm and aluminum foil, which were perforated with holes. The films were further dried in a desiccator for 4–16 h to remove residual solvent while protected from light. The dried lipid films were hydrated in Tris-buffered saline (TBS) [50 mM Tris pH 8.0 (4°C) and 200 mM NaCl] at a final concentration of 10 mM total for the solvating lipid and 0.12 mM for 16:0 Liss Rhod PE and vortexed ~5 min until the film was dissolved. Next, the opaque lipid mixtures were sonicated for 30 mins at 40°C until clear. In a total volume of 100 μL, lipids containing Liss Rhod PE were mixed at a final concentration of 1 mM with neutralized AASTY polymer solution at a final concentration of 1 wt % in TBS. The samples were incubated for 2 h at 4°C under gentle agitation. Non-solubilized lipids were removed by ultracentrifugation at 90,000 × g for 10 min. The supernatant was run through a 0.22 μm spin filter unit before being injected onto a Superose 6 Increase 5/150 GL column equilibrated with TBS. The separation was performed at a flow rate of 0.2 mL/min and the eluent was detected by a Shimadzu fluorometer with an excitation wavelength of 554 nm, emission of 576 nm for detection of Liss Rhod PE and a recording time of 20 min.

Preparation of hTRPM4 in AASTY Nanodiscs

hTRPM4 fused with an N-terminal StrepTagII-eGFP tag was expressed in HEK293F cells using the baculovirus expression system as described by Autzen et al.[36] In short, 850 mL suspension HEK293F culture was transferred to a 1 L spin tube and ten 2 mL centrifuge tubes 48 h after transduction. hTRPM4 was expressed at 37°C and enhanced with 10 mM sodium butyrate 24 h after transduction. The large pellet was then resuspended in 20 mL TBS supplemented with an EDTA-free SIGMAFAST protease inhibitor cocktail tablet (Sigma), split in two 50 mL centrifugation tubes (~5 g in each), snap frozen in liquid N_2, and stored at −80°C until further use. The 2 mL centrifuge tube pellets (~12 mg each) were isolated from the media and snap frozen directly. hTRPM4 was extracted from HEK293F cells with AASTY polymers and analyzed either as a crude lysate in FSEC for initial copolymer screening or was purified with affinity chromatography and SEC.

FSEC with hTRPM4 in AASTY Nanodiscs

Each 2 mL centrifuge tube with HEK293F cells expressing hTRPM4 were thawed and resuspended in 200 μL TBS supplemented with EDTA-free SIGMAFAST protease inhibitor cocktail tablets (Sigma). 50 μL of the cell suspension was mixed with 50 μL 4% (w/v) polymer solubilized in TBS for a final concentration of 2% (w/v) and incubated on a rolling table for 2 h at 4°C. Large aggregates were removed from the suspension by ultracentrifugation at 90.000 × g for 10 min and the supernatant was filtered with a 0.22 μm spin filter unit before 10 μL sample was loaded onto a Superose 6 Increase 5/150 GL column pre-equilibrated with TBS buffer. The separation was performed at a flow rate of 0.2 mL/min and the eluent was detected by a Shimadzu fluorometer with an excitation wavelength of 488 nm, emission of 509 nm for detection of eGFP and a recording time of 20 min.

Purification of hTRPM4 in AASTY-B Nanodiscs

The 5 g HEK293F pellets with hTRPM4 were thawed and incubated with Buffer A (50 mM HEPES 7.4, 150 mM NaCl) supplemented with ASSTY polymer In a final volume of 45 mL and 1.5% (w/v) of the polymer for 2 h on a rolling table at 4°C. Large aggregates were removed from the suspension by low-speed centrifugation at 26,000 × g for 30 min. The supernatant was then transferred to 1 mL Buffer A equilibrated StrepTactin beads (GE Life Sciences) and incubated overnight to allow binding of the StrepTagII-tagged hTRPM4 (14 h) upon addition of L-Arg-HCl (buffered to pH 7.4) to a final concentration of 250 mM. Unbound material was washed off with 30 column volumes (CV) Buffer B

(Buffer A supplemented with 250 mM L-Arg) and the protein was eluted with 2 CV Buffer C (Buffer B with 5 mM D-desthiobiotin). The eluted protein was concentrated to ~4 mg/mL as assessed by a NanoDrop UV-vis spectrophotometer (280 nm, 1 mg = 1 Abs) on Amicon Ultra 4 mL Centrifugal Filters. Next, the sample was filtered with a 0.22 μm spin filter after which 450 uL was injected onto a Superose 6 Increase 10/300 GL column equilibrated with Buffer A. Peak fractions were pooled and concentrated to 2 mg/mL. The purity and quality of the ASSTY encircled hTRPM4 was assessed by SDS-PAGE, negative stain, and single-particle cryo-EM.

EM Sample Preparation and Data Acquisition

Grids of hTRPM4 in ASSTY nanodiscs were prepared by applying 3 μL of the sample (2 mg/mL, NanoDrop 280 nm, 1 Abs = 1 mg/mL) to a glow-discharged Quantifoil R1.2/1.3 300-mesh Au holey carbon grid (Quantifoil, micro tools). The grids were plunge-frozen in liquid ethane using a Vitrobot Mark IV (FEI) with a blotting time of 7 s, blot force of 3°C at 10°C and at 100% humidity using Whatman Grade 1 filter paper. Data sets were collected on a FEI Talos Arctica (Thermo Fisher Scientific, US) operated at 200 kV and equipped with an X-FEG electron source. Images were recorded in super-resolution mode at a nominal magnification of 36,000× corresponding to a physical pixel size of 1.14 Å at the specimen level and a K3 Summit direct electron detector (Gatan, US). The defocus range was set to 0.5–2.0 μm under focus. Total exposure of 3.2 s was used with a 0.04 s frame rate (80 total frames).

Image Processing

Dose-fractionated super-resolution image stacks were motion corrected and binned by a factor of two by Fourier cropping using MotionCor2.[53] Motion corrected sums with dose weighting were used for contrast transfer function (CTF) determination using CTFFIND4[54] in *cis*TEM.[55] Reference free particle picking was done in *cis*TEM. A total of 172,315 particles were selected from 548 micrographs and exported to cryoSPARC[56,57] using scripts from the UCSF pyem module.[58] After two rounds of 2D classifications, 42,500 particles were used for further processing in 3D without imposing symmetry. For refinement, a previously solved structure of hTRPM4 without symmetry was low-pass filtered to 30 Å and used as the reference model.

Quantification and Statistical Analysis

The polymers were simulated using the compositional drift analysis tool, which facilitates visualization of the monomer run-length distribution, while also calculating the λ-factor, allowing a numerical readout for the alternating behavior of the polymers and a comparison of their structures.[46]

Additional Resources

The compositional drift program used in this study can be found here: https://github.com/vince-wu/CompositionalDrift.

SUPPLEMENTAL INFORMATION

Supplemental Information can be found online at https://doi.org/10.1016/j.chempr.2020.08.004.

Chem
Article

🔁 CellPress

AUTHOR CONTRIBUTIONS

DECLARATION OF INTERESTS

REFERENCES

1. Autzen, H.E., Julius, D., and Cheng, Y. (2019). Membrane mimetic systems in cryoEM: keeping membrane proteins in their native environment. Curr. Opin. Struct. Biol. 58, 259–268.

2. Denisov, I.G., and Sligar, S.G. (2017). Nanodiscs in membrane biochemistry and biophysics. Chem. Rev. 117, 4669–4713.

3. Marty, M.T., Hoi, K.K., Gault, J., and Robinson, C.V. (2016). Probing the lipid annular belt by gas-phase dissociation of membrane proteins in nanodiscs. Angew. Chem. Int. Ed. 55, 550–554.

4. Lee, S.C., Knowles, T.J., Postis, V.L.G., Jamshad, M., Parslow, R.A., Lin, Y.P., Goldman, A., Sridhar, P., Overduin, M., Muench, S.P., and Dafforn, T.R. (2016). A method for detergent-free isolation of membrane proteins in their local lipid environment. Nat. Protoc. 11, 1149–1162.

5. Sun, C., Benlekbir, S., Venkatakrishnan, P., Wang, Y.H., Hong, S.J., Hosler, J., Tajkhorshid, E., Rubinstein, J.L., and Gennis, R.B. (2018). Structure of the alternative complex III in a supercomplex with cytochrome oxidase. Nature 557, 123–126.

6. Qiu, W.H., Fu, Z., Xu, G.G., Grassucci, R.A., Zhang, Y., Frank, J., Hendrickson, W.A., and Guo, Y.Z. (2018). Structure and activity of lipid bilayer within a membrane-protein transporter. Proc. Natl. Acad. Sci. USA 115, 12985–12990.

7. Parmar, M., Rawson, S., Scarff, C.A., Goldman, A., Dafforn, T.R., Muench, S.P., and Postis, V.L.G. (2018). Using a SMALP platform to determine a sub-nm single particle cryo-EM membrane protein structure. Biochim. Biophys. Acta Rev. Biomembr. 1860, 378–383.

8. Karlova, M.G., Voskoboynikova, N., Gluhov, G.S., Abramochkin, D., Malak, O.A., Mulkidzhanyan, A., Loussouarn, G., Steinhoff, H.J., Shaitan, K.V., and Sokolova, O.S. (2019). Detergent-free solubilization of human Kv channels expressed in mammalian cells. Chem. Phys. Lipids 219, 50–57.

9. Yoder, N., and Gouaux, E. (2020). Conserved His-Gly motif of acid-sensing ion channels resides in a reentrant 'loop' implicated in gating and ion selectivity. bioRxiv. biorxiv.org/content/10.1101/2020.03.02.974154v1.

10. Yu, J., Zhu, H., Lape, R., Greiner, T., Shahoei, R., Wang, Y., Du, J., Lü, W., Tajkhorshid, E., Sivilotti, L., and Gouaux, E. (2019). Mechanism of gating and partial agonist action in the glycine receptor. bioRxiv. biorxiv.org/content/10.1101/786632v1.

11. Scheidelaar, S., Koorengevel, M.C., van Walree, C.A., Dominguez, J.J., Dörr, J.M., and Killian, J.A. (2016). Effect of polymer composition and pH on membrane solubilization by styrene-maleic acid copolymers. Biophys. J. 111, 1974–1986.

12. Burridge, K.M., Harding, B.D., Sahu, I.D., Kearns, M.M., Stowe, R.B., Dolan, M.T., Edelmann, R.E., Dabney-Smith, C., Page, R.C., Konkolewicz, D., and Lorigan, G.A. (2020). Simple derivatization of RAFT-synthesized styrene-maleic anhydride copolymers for lipid disc formulations. Biomacromolecules 21, 1274–1284.

13. Ravula, T., Ramadugu, S.K., Di Mauro, G., and Ramamoorthy, A. (2017). Bioinspired, size-tunable self-assembly of polymer-lipid bilayer nanodiscs. Angew. Chem. Int. Ed. 56, 11466–11470.

14. Lindhoud, S., Carvalho, V., Pronk, J.W., and Aubin-Tam, M.E. (2016). SMA-SH: modified styrene-maleic acid copolymer for functionalization of lipid nanodiscs. Biomacromolecules 17, 1516–1522.

15. Hall, S.C.L., Tognoloni, C., Charlton, J., Bragginton, É.C., Rothnie, A.J., Sridhar, P., Wheatley, M., Knowles, T.J., Arnold, T., Edler, K.J., and Dafforn, T.R. (2018). An acid-compatible co-polymer for the solubilization of membranes and proteins into lipid bilayer-containing nanoparticles. Nanoscale 10, 10609–10619.

16. Ravula, T., Hardin, N.Z., Di Mauro, G.M., and Ramamoorthy, A. (2018). Styrene maleic acid derivates to enhance the applications of bio-inspired polymer based lipid-nanodiscs. Eur. Polym. J. 108, 597–602.

17. Ravula, T., Hardin, N.Z., Ramadugu, S.K., Cox, S.J., and Ramamoorthy, A. (2018). Formation of pH-resistant monodispersed polymer–lipid nanodiscs. Angew. Chem. Int. Ed. 57, 1342–1345.

18. Overduin, M., and Esmaili, M. (2019). Native nanodiscs and the convergence of lipidomics, metabolomics, interactomics and proteomics. Appl. Sci. 9, 1230.

19. Stroud, Z., Hall, S.C.L., and Dafforn, T.R. (2018). Purification of membrane proteins free from conventional detergents: SMA, new polymers, new opportunities and new insights. Methods 147, 106–117.

20. Lee, S.C., and Pollock, N.L. (2016). Membrane proteins: is the future disc shaped? Biochem. Soc. Trans. 44, 1011–1018.

21. Smith, A.A.A., Autzen, H.E., Laursen, T., Wu, V., Yen, M., Hall, A., Hansen, S.D., Cheng, Y.F., and Xu, T. (2017). Controlling styrene maleic acid lipid particles through RAFT. Biomacromolecules 18, 3706–3713.

22. Hall, S.C.L., Tognoloni, C., Price, G.J., Klumperman, B., Edler, K.J., Dafforn, T.R., and Arnold, T. (2018). Influence of Poly(styrene-co-maleic acid) Copolymer Structure on the Properties and Self-Assembly of SMALP nanodiscs. Biomacromolecules 19, 761–772.

23. Bada Juarez, J.F.B., Harper, A.J., Judge, P.J., Tonge, S.R., and Watts, A. (2019). From polymer chemistry to structural biology: the development of SMA and related amphipathic polymers for membrane protein extraction and solubilisation. Chem. Phys. Lipids 221, 167–175.

24. Sun, C., and Gennis, R.B. (2019). Single-particle cryo-EM studies of transmembrane proteins in SMA copolymer nanodiscs. Chem. Phys. Lipids 221, 114–119.

25. Klumperman, B. (2010). Mechanistic considerations on styrene-maleic anhydride

copolymerization reactions. Polym. Chem. *1*, 558–562.

26. Yao, Z., Li, B.G., Wang, W.J., and Pan, Z.R. (1999). Continuous thermal bulk copolymerization of styrene and maleic anhydride. J. Appl. Polym. Sci. *73*, 615–622.

27. Harrisson, S., Ercole, F., and Muir, B.W. (2010). Living spontaneous gradient copolymers of acrylic acid and styrene: one-pot synthesis of pH-responsive amphiphiles. Polym. Chem. *1*, 326–332.

28. Zoonens, M., and Popot, J.L. (2014). Amphipols for each season. J. Membr. Biol. *247*, 759–796.

29. Hardin, N.Z., Ravula, T., Mauro, G.D., and Ramamoorthy, A. (2019). Hydrophobic functionalization of polyacrylic acid as a versatile platform for the development of polymer lipid nanodisks. Small *15*, e1804813.

30. Yasuhara, K., Arakida, J., Ravula, T., Ramadugu, S.K., Sahoo, B., Kikuchi, J.I., and Ramamoorthy, A. (2017). Spontaneous lipid nanodisc fomation by amphiphilic polymethacrylate copolymers. J. Am. Chem. Soc. *139*, 18657–18663.

31. Hardy, D., Bill, R.M., Rothnie, A.J., and Jawhari, A. (2019). Stabilization of human multidrug resistance Protein 4 (MRP4/ABCC4) using novel solubilization agents. SLAS Discov. *24*, 1009–1017.

32. Gulamhussein, A.A., Meah, D., Soja, D.D., Fenner, S., Saidani, Z., Akram, A., Lallie, S., Mathews, A., Painter, C., Liddar, M.K., et al. (2019). Examining the stability of membrane proteins within SMALPs. Eur. Polym. J. *112*, 120–125.

33. Dörr, J.M., Koorengevel, M.C., Schäfer, M., Prokofyev, A.V., Scheidelaar, S., van der Cruijsen, E.A.W., Dafforn, T.R., Baldus, M., and Killian, J.A. (2014). Detergent-free isolation, characterization, and functional reconstitution of a tetrameric K+ channel: the power of native nanodiscs. Proc. Natl. Acad. Sci. USA *111*, 18607–18612.

34. Gulamhussein, A.A., Uddin, R., Tighe, B.J., Poyner, D.R., and Rothnie, A.J. (2020). A comparison of SMA (styrene maleic acid) and DIBMA (di-isobutylene maleic acid) for membrane protein purification. Biochim. Biophys. Acta Rev. Biomembr. *1862*, 183281.

35. Fiori, M.C., Zheng, W., Kamilar, E., Simiyu, G., Altenberg, G.A., and Liang, H. (2020). Extraction and reconstitution of membrane proteins into lipid nanodiscs encased by zwitterionic styrene-maleic amide copolymers. Sci. Rep. *10*, 9940.

36. Autzen, H.E., Myasnikov, A.G., Campbell, M.G., Asarnow, D., Julius, D., and Cheng, Y. (2018). Structure of the human TRPM4 ion channel in a lipid nanodisc. Science *359*, 228–232.

37. Oluwole, A.O., Danielczak, B., Meister, A., Babalola, J.O., Vargas, C., and Keller, S. (2017). Solubilization of membrane proteins into functional lipid-bilayer nanodiscs using a diisobutylene/maleic acid copolymer. Angew. Chem. Int. Ed. *56*, 1919–1924.

38. Burgess, J., and Drasdo, D.N. (1993). Solubilities of calcium salts of dicarboxylic acids in methanol-water mixtures; transfer chemical potentials of dicarboxylate anions. Polyhedron *12*, 2905–2911.

39. Mitrofanova, G.V. (2002). Complexation of calcium ions with dicarboxylic acids in aqueous solutions. Russ. J. Appl. Chem. *75*, 712–714.

40. Teo, A.C.K., Lee, S.C., Pollock, N.L., Stroud, Z., Hall, S., Thakker, A., Pitt, A.R., Dafforn, T.R., Spickett, C.M., and Roper, D.I. (2019). Analysis of SMALP co-extracted phospholipids shows distinct membrane environments for three classes of bacterial membrane protein. Sci. Rep. *9*, 1813.

41. Dominguez Pardo, J.J.D., Dörr, J.M., Iyer, A., Cox, R.C., Scheidelaar, S., Koorengevel, M.C., Subramaniam, V., and Killian, J.A. (2017). Solubilization of lipids and lipid phases by the styrene-maleic acid copolymer. Eur. Biophys. J. *46*, 91–101.

42. Scheidelaar, S., Koorengevel, M.C., Pardo, J.D., Meeldijk, J.D., Breukink, E., and Killian, J.A. (2015). Molecular model for the solubilization of membranes into nanodisks by styrene maleic acid copolymers. Biophys. J. *108*, 279–290.

43. Subczynski, W.K., Pasenkiewicz-Gierula, M., Widomska, J., Mainali, L., and Raguz, M. (2017). High cholesterol/low cholesterol: effects in biological membranes: a review. Cell Biochem. Biophys. *75*, 369–385.

44. van Meer, G., Voelker, D.R., and Feigenson, G.W. (2008). Membrane lipids: where they are and how they behave. Nat. Rev. Mol. Cell Biol. *9*, 112–124.

45. Domínguez Pardo, J.J.D., Koorengevel, M.C., Uwugiaren, N., Weijers, J., Kopf, A.H., Jahn, H., van Walree, C.A., van Steenbergen, M.J., and Killian, J.A. (2018). Membrane solubilization by styrene-maleic acid copolymers: delineating the role of polymer length. Biophys. J. *115*, 129–138.

46. Smith, A.A.A., Hall, A., Wu, V., and Xu, T. (2019). Practical prediction of heteropolymer composition and drift. ACS Macro Lett. *8*, 36–40.

47. Fredrickson, G.H., Milner, S.T., and Leibler, L. (1992). Multicritical phenomena and microphase ordering in random block copolymers melts. Macromolecules *25*, 6341–6354.

48. Duan, J., Li, J., Zeng, B., Chen, G.L., Peng, X., Zhang, Y., Wang, J., Clapham, D.E., Li, Z., and Zhang, J. (2018). Structure of the mouse TRPC4 ion channel. Nat. Commun. *9*, 3102.

49. Duan, J., Li, Z., Li, J., Santa-Cruz, A., Sanchez-Martinez, S., Zhang, J., and Clapham, D.E. (2018). Structure of full-length human TRPM4. Proc. Natl. Acad. Sci. USA *115*, 2377–2382.

50. Winkler, P.A., Huang, Y., Sun, W., Du, J., and Lü, W. (2017). Electron cryo-microscopy structure of a human TRPM4 channel. Nature *552*, 200–204.

51. Augustyn, B., Stepien, P., Poojari, C., Mobarak, E., Polit, A., Wisniewska-Becker, A., and Róg, T. (2019). Cholesteryl hemisuccinate is not a good replacement for cholesterol in lipid nanodiscs. J. Phys. Chem. B *123*, 9839–9845.

52. Jesson, C.P., Pearce, C.M., Simon, H., Werner, A., Cunningham, V.J., Lovett, J.R., Smallridge, M.J., Warren, N.J., and Armes, S.P. (2017). H$_2$O$_2$ Enables convenient removal of RAFT end-groups from block copolymer nano-objects prepared via polymerization-induced self-assembly in water. Macromolecules *50*, 182–191.

53. Zheng, S.Q., Palovcak, E., Armache, J.P., Verba, K.A., Cheng, Y.F., and Agard, D.A. (2017). MotionCor2: anisotropic correction of beam-induced motion for improved cryo-electron microscopy. Nat. Methods *14*, 331–332.

54. Rohou, A., and Grigorieff, N. (2015). CTFFIND4: fast and accurate defocus estimation from electron micrographs. J. Struct. Biol. *192*, 216–221.

55. Grant, T., Rohou, A., and Grigorieff, N. (2018). cisTEM, user-friendly software for single-particle image processing. eLife *7*, e35383.

56. Punjani, A., Rubinstein, J.L., Fleet, D.J., and Brubaker, M.A. (2017). cryoSPARC: algorithms for rapid unsupervised cryo-EM structure determination. Nat. Methods *14*, 290–296.

57. Scheres, S.H. (2012). RELION: implementation of a Bayesian approach to cryo-EM structure determination. J. Struct. Biol. *180*, 519–530.

58. Asarnow, D., Palovcak, E., and Cheng, Y. (2019). asarnow/pyem: UCSF pyem v0.5. Zendo. https://doi.org/10.5281/zenodo.3576630.

59. Pettersen, E.F., Goddard, T.D., Huang, C.C., Couch, G.S., Greenblatt, D.M., Meng, E.C., and Ferrin, T.E. (2004). UCSF Chimera—a visualization system for exploratory research and analysis. J. Comput. Chem. *25*, 1605–1612.

Supplemental Information

Lipid Nanodiscs via Ordered Copolymers

Anton A.A. Smith, Henriette E. Autzen, Bryan Faust, Joseph L. Mann, Benjamin W. Muir, Shaun Howard, Almar Postma, Andrew J. Spakowitz, Yifan Cheng, and Eric A. Appel
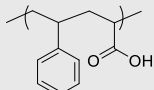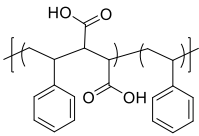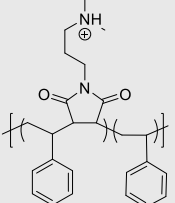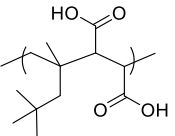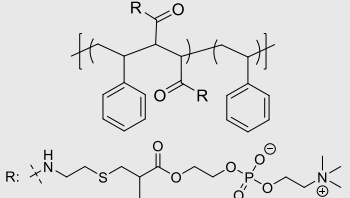
Lipid Nanodiscs via Ordered Copolymers

Anton A. A. Smith,[+] Henriette E. Autzen,[+] Bryan Faust, Joseph L. Mann. Benjamin W. Muir Shaun Howard, Almar Postma, Andrew J. Spakowitz, Yifan Cheng*, and Eric A. Appel*

Table S1. Solubilization efficacy in comparison to SMA2000, along with buffer restrictions for polymers.

Polymers	Ca^{2+} tolerance	pH range	Efficacy*	Reference
AASTY	6 mM	6.5+	5-10	This work
SMA2000	2 mM	6.5+	1	1
SMI	100+ mM	all ranges	<1	2
DIBMA	up to 30 mM	6.5+	0.5	3
zSMA	N/A	all ranges	~3	2

* Efficacy is given as relative to SMA2000. Note that each comparison is for a specific system in the given reference. 123
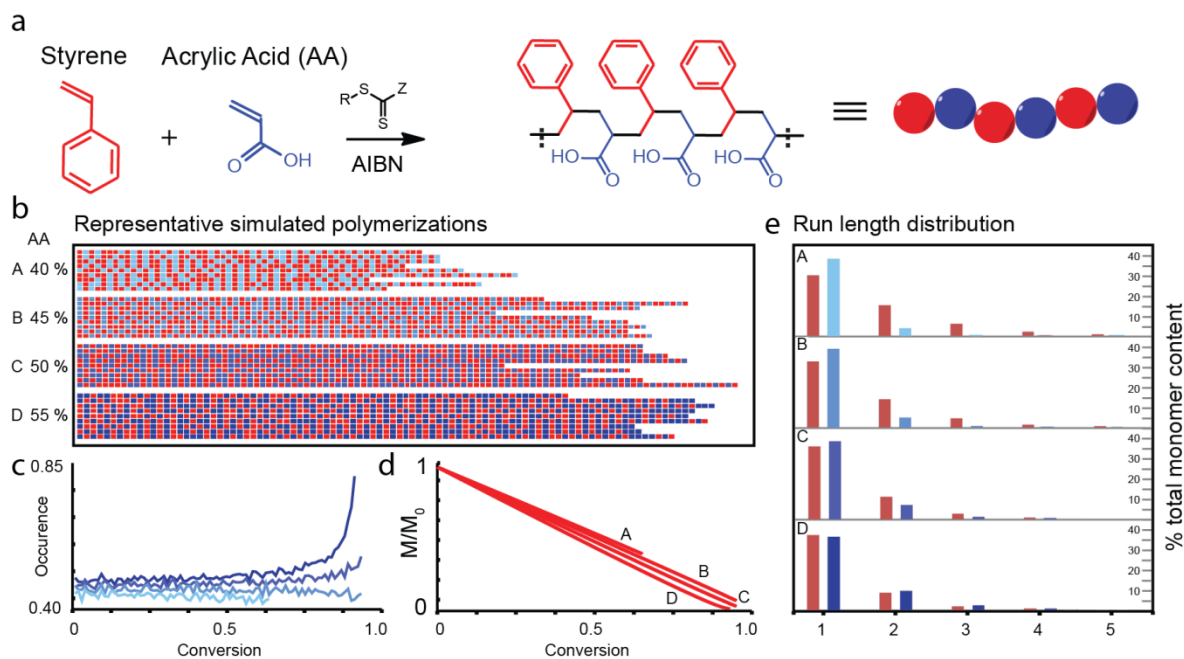
Figure S1. Compositional drift analysis of AASTY copolymers A-D. a) Reaction of styrene and acrylic acid, with colors symbolizing styrene (red) and acrylic acid (blue) in the subsequent panels. b-e) Simulation of polymer compositions of A (40% initial AA), B (45 % initial AA), C (50% initial AA), and D (55% initial AA), at the measured conversions. b) Examples of simulated chains, with each row representing one polymer. c) Probability of styrene being consumed at a given global conversion. d) Consumption of AA, as a function of global monomer conversion. e) Distribution of run lengths for styrene and acrylic acid for each polymerization.

AASTY and DDM-CHS hTRPM4 solubilization
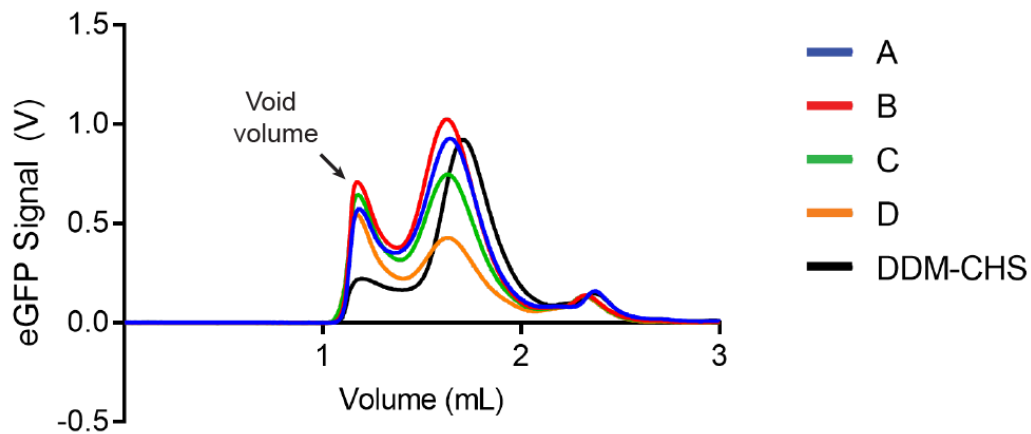
Figure S2. Comparison of extraction efficiency of hTRMP4 with the AASTY polymers and DDM-CHS. Raw FSEC traces of solubilizing the eGFP-tagged hTRPM4 extracted from HEK293 cells in the four AASTY polymers and DDM-CHS. The void volume and the peak with properly folded protein are marked with arrows. The experiments were conducted using cell pellets from the same batch of transduced cultures and with the same suspension, solubilization and injection volumes, and on the same SEC column. FSEC of AASTY and DDM-CHS were performed on two concomitant days to keep the timing of each individual step consistent between experiments.
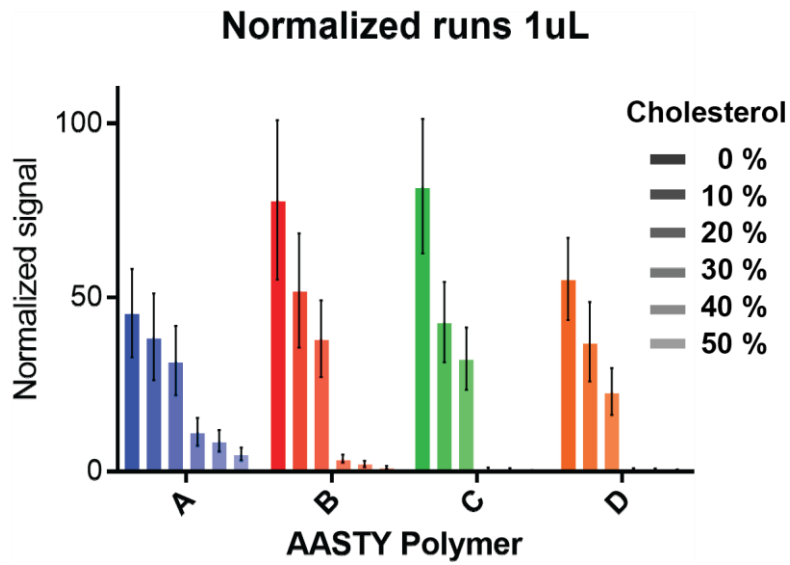
Figure S3. Effect of cholesterol on nanodisc formation from lipid vesicles. Maximum fluorescence signals from FSEC with polymers A, B, C and D and various ratios of POPC and cholesterol with an overall increase in the content of cholesterol, increasing from 0-50% in 10% increments by weight, going left to right for each polymer, while keeping a constant 2 % Liss Rhod PE. Values are normalized relative to the highest detected signal within the represented data and error bars represent the standard deviation between three injections of the same sample.
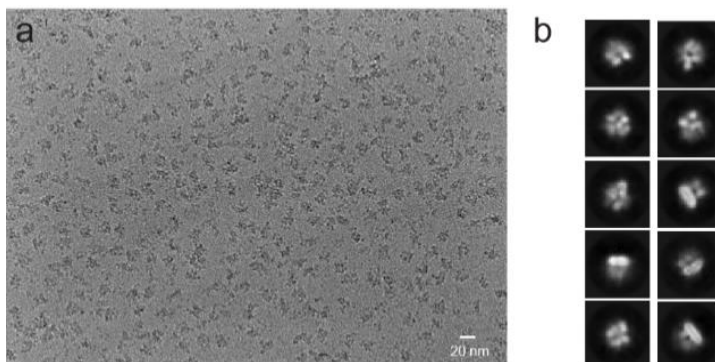
Figure S4: Representative single-particle cryo-EM micrograph of hTRPM4 in AASTY-B a) on a GO grid. b) 2D class averages of hTRPM4 picked from micrographs as in a).

1.   Hall, S.C.L., Tognoloni, C., Charlton, J., Bragginton, E.C., Rothnie, A.J., Sridhar, P., Wheatley, M., Knowles, T.J., Arnold, T., Edler, K.J.*, et al.* (2018). An acid-compatible co-polymer for the solubilization of membranes and proteins into lipid bilayer-containing nanoparticles. Nanoscale *10*, 10609-10619.

2.   Gulamhussein, A.A., Uddin, R., Tighe, B.J., Poyner, D.R., and Rothnie, A.J. (2020). A comparison of SMA (styrene maleic acid) and DIBMA (di-isobutylene maleic acid) for membrane protein purification. Bba-Biomembranes *1862*.

3.   Fiori, M.C., Zheng, W., Kamilar, E., Simiyu, G., Altenberg, G.A., and Liang, H. (2020). Extraction and reconstitution of membrane proteins into lipid nanodiscs encased by zwitterionic styrene-maleic amide copolymers. Sci Rep-Uk *10*, 9940.